#164

Rupture Velocity Dependence of Fracture Energy for Sub-Rayleigh Ruptures on a 6-Meter-Long Laboratory Fault

Kurama Okubo[1]; Futoshi Yamashita[1]; Yoshiaki Matsumoto[1]; Eiichi Fukuyama[2, 1]

[1]National Research Institute for Earth Science and Disaster Resilience (NIED) (kokubo@bosai.go.jp), [2]Graduate School of Engineering, Kyoto University

1. Abstract

Fracture energy governs key aspects of earthquake ruptures, including critical nucleation length, rupture acceleration, termination, and the energy budget (Palmer & Rice, 1973; Weng & Ampuero, 2022; Ke et al., 2018; Cocco et al., 2023). Evaluating this parameter in large-scale laboratory experiments is essential for quantifying the rupture dynamics of laboratory earthquakes. Here, we estimated fracture energy using a 6-meter biaxial rock-friction apparatus by fitting a steady-state rupture model with a linear cohesive zone (Poliakov et al., 2002) to local shear stress changes recorded 15 mm from the fault surface. Rupture velocity was determined from time shifts of neighboring shear stress histories and used to constrain local estimates of fracture energy (Γ) and cohesive-zone size (X_c). Fracture energy decreased from 0.07 to 0.005 J/m² as rupture velocity approached the Rayleigh speed (c_R) in sub-Rayleigh ruptures, which may be consistent with dynamic rupture theory (Freund, 1990) that predicts vanishing fracture energy near the limiting speed.

2. Introduction

Figure 1: Photograph of the 6-meter-long biaxial rock-friction apparatus. The upper and lower metagabbro specimens (yellow box) are vertically stacked within the outer frame. Their dimensions are L = 6.0 m, W = 0.5 m, H = 0.75 m (upper) and L = 7.5 m, W = 0.5 m, H = 0.75 m (lower). Six independently servo-controlled normal-load jacks allow controlled rupture nucleation by locally reducing the normal load following shear loading. Semiconductor strain gauges were installed 15 mm from the fault at 130-mm spacing on both the north and south sides (inset). Strain data were recorded continuously at 1 MHz with 16-bit resolution.

Although fracture energy is a key parameter for characterizing rupture dynamics, its measurement remains technically challenging, particularly in large-scale experiments. One approach is to evaluate it directly from shear stress–slip histories (e.g., Ohnaka, 2003), but this was difficult in large-scale experiments because slip sensors have a limited measurement range and strain gauges cannot be installed close enough to the fault (Xu et al., 2019).

A practical alternative is to use the dynamic stress field around the rupture front, inferring fracture energy by fitting rupture models to off-fault shear stress histories (e.g., Svetlizky et al., 2017; Kammer & McLaskey, 2019). We apply this approach to a new 6-m biaxial rock-friction apparatus at NIED (Figure 1) to estimate fracture energy and examine its variation at rupture velocities near the Rayleigh wave velocity, c_R, providing insight into the energy balance of earthquakes with ruptures propagating near the limiting speed.

3. Methodology

3.1 Nucleation-Controlled Laboratory Earthquake Events

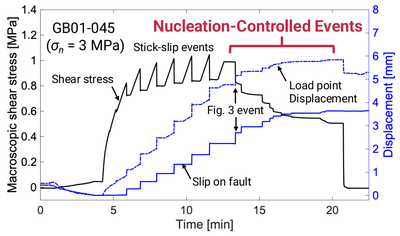

Figure 2: Time histories of macroscopic shear stress measured by the shear loading jack, shear load point displacement, and cumulative slip on the simulated fault obtained from a laser displacement sensor at the eastern edge of the fault.

We conducted stick–slip experiments by applying a normal stress of 3 MPa, with shear loading applied under displacement control at 0.01 mm/s. Subsequently, the load on one of the normal jacks was reduced to control the nucleation location and timing of the events (Figure 2). We analyzed these nucleation-controlled events.

3.2 Dynamic Stress Field Near the Rupture Front

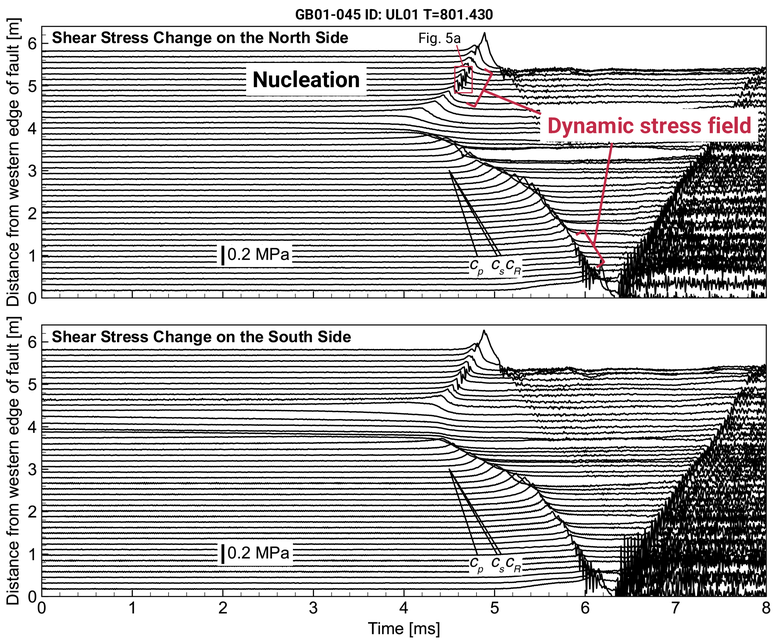

Figure 3: Shear stress changes associated with one of the nucleation-controlled events. Black traces show local shear stress records 15 mm from the fault at different positions (low-pass filtered at 60 kHz). The stress field near the rupture front (red) is used to estimate the fracture energy and the characteristic slip distance.

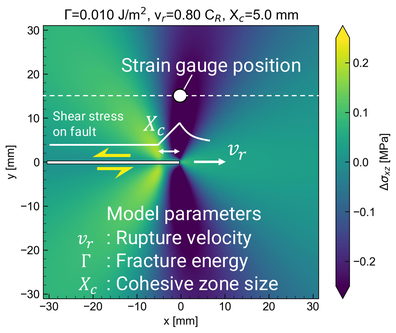

Figure 4: Spatial distribution of the shear stress change around the rupture front with the linear cohesive-zone rupture model.

We analyzed near-fault shear stress histories from three nucleation-controlled events. Figure 3 presents one example, nucleated near the reduced normal load (NL4 in Figure 1), which propagated bilaterally with rupture velocity approaching c_R. Fracture energy (Γ) and cohesive-zone size (X_c) were locally evaluated by searching for the best-fit parameters of a linear cohesive-zone rupture model (Figure 4) that reproduce the observed shear stress histories (Figure 5b).

4. Results

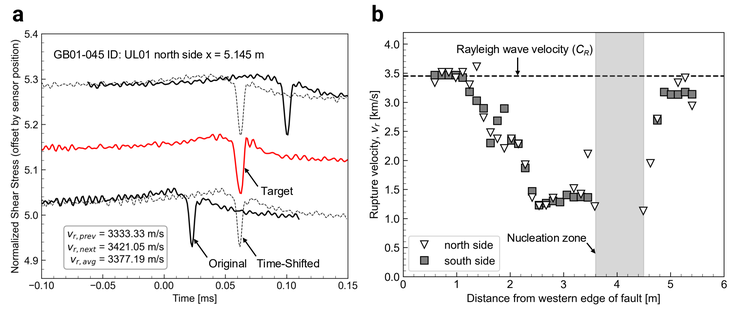

Figure 5: Estimation of local rupture velocity. (a) Evaluation based on the time lags obtained by cross-correlation of neighboring shear stress histories. (b) Estimated rupture velocity distribution along the simulated fault. The gray band indicates the nucleation zone, and the dashed line shows the Rayleigh wave speed c_R.

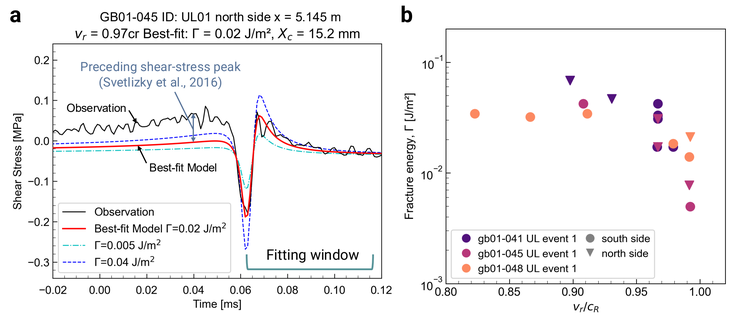

Figure 6: Estimation of fracture energy. (a) Example of model fitting to the observed shear stress history. The red line indicates the best-fit model, while the blue and cyan lines represent models with different assumed fracture energies. (b) The fracture energy (Γ) estimates constrained for rupture velocities between 0.8 c_R and 0.99 c_R.

The rupture velocity at the target position was obtained by averaging the velocity estimates from the two adjacent sensors (Figures 5a and 5b). With the rupture velocity fixed, the fracture energy (Γ) and the cohesive-zone size (X_c) were optimized by grid search to minimize the root-mean-square error (RMSE) (Figure 6a), using a fitting window after the negative stress peak to avoid misfit due to artifacts (Svetlizky et al., 2016). The estimated fracture energy showed the trend that decreased from 0.07 to 0.005 J/m² as rupture velocity approached c_R (Figure 6b).

5. Discussion

The estimated fracture energy lies at the lower bound of previous estimates on gabbro faults (Kammer and McLaskey, 2019), which may reflect the smoother fault surface in our experiments. Decrease in the fracture energy with increasing the rupture velocity may be explained by dynamic fracture theory based on linear elastic fracture mechanics (LEFM) (Freund, 1990; Svetlizky et al., 2017). Ongoing work includes increasing the number of analyzed events to improve the statistical robustness of the model parameters and clarifying the theoretical framework needed to explain the energy balance at high rupture velocities.

6. Conclusions

- The 6-m laboratory fault reproduces the rupture propagation near c_R.
- Fracture energy decreases from 0.07 to 0.005 J/m² as rupture velocity approaches c_R.
- This trend may reflect dynamic fracture theory based on LEFM, but more robust statistics are needed to clarify the energy balance.

References

Cocco et al. (2023). https://doi.org/10.1146/annurev-earth-071822-100304
Freund, L. B. (1990). https://doi.org/10.1017/CBO9780511546761
Kammer, D. and McLaskey, G. (2019). https://doi.org/10.1016/j.epsl.2019.01.031
Ke, C.-Y., McLaskey, G. C., and Kammer, D. S. (2018). https://doi.org/10.1029/2018GL080492
Ohnaka, M. (2003). https://doi.org/10.1029/2000JB000123
Palmer, A. C. and Rice, J. R. (1973). https://doi.org/10.1098/rspa.1973.0040
Poliakov, A. N., Dmowska, R., and Rice, J. R. (2002). https://doi.org/10.1029/2001JB000572
Svetlizky, I. et al. (2016). https://doi.org/10.1073/pnas.1517545113
Svetlizky, I. et al. (2017). https://doi.org/10.1103/PhysRevLett.118.125501
Weng, H. and Ampuero, J.-P. (2022). https://doi.org/10.1038/s41467-022-34927-w
Xu, S., Fukuyama, E., and Yamashita, F. (2019). https://doi.org/10.1029/2018JB016797